Available online at www.sciencedirect.com
ScienceDirect
Journal of Nuclear Materials 356 (2006) 1–15
journal of nuclear materials
www.elsevier.com/locate/jnucmat

Status of the Spallation Neutron Source with focus on target materials

L.K. Mansur *, J.R. Haines

Oak Ridge National Laboratory, Oak Ridge, TN 37831, USA

Abstract

An overview of the design and construction of the Spallation Neutron Source (SNS) is presented. Key facility performance parameters are summarized and plans for initial operation are described. Early efforts produced a conceptual design in 1997; the project itself was initiated in 1999, with the official groundbreaking taking place in December of 1999. As of April 2005 building construction was complete and the overall project was more than 90% complete. The design of the target and surrounds are finished and the first target was installed in June 2005. First beam on target is expected in June, 2006. The engineering design of the target region is described. The key systems comprise the mercury target, moderator and reflector assemblies, remote handling systems, utilities and shielding. Through interactions with the 1 GeV proton beam, the target, moderators and reflectors produce short pulse neutrons in thermal energy ranges, which are transported to a variety of neutron scattering instruments. The mercury target module itself is described in more detail. Materials issues are expected to govern the overall lifetime and have influenced the design, fabrication and planned operation. A wide range of materials research and development has been carried out to provide experimental data and analyses to ensure the satisfactory performance of the target and to set initial design conditions. Materials R&D concentrated mainly on cavitation erosion, radiation effects, and mercury compatibility issues, including investigations of the mechanical properties during exposure to mercury. Questions that would require future materials research are discussed.
Published by Elsevier B.V.

1. Introduction

Early plans to design and build a new high power accelerator-based neutron source for neutron science research were underway at Oak Ridge National Laboratory in 1994 and 1995. Discussions of alternative concepts were centered in two areas, the proton accelerator system and the neutron spallation target. The system contemplated was a short pulse facility in the megawatt power range, so it was clear that the type and characteristics of the target would need careful consideration. This component would present a number of issues to be solved, including materials behavior and power handling. In particular, radiation damage to target materials was an early focus because there were only sparse data on radiation damage by GeV range protons and the resulting spallation neutrons, meaning that the response to irradiation of the structural materials was uncertain [1–3]. Additional materials questions centered on the compatibility of the target container with the coolant for a liquid-cooled solid

* Corresponding author. Tel.: +1 865 574 4797; fax: +1 865 24 3650.
E-mail address: mansurlk@ornl.gov (L.K. Mansur).

0022-3115/$ - see front matter Published by Elsevier B.V.
doi:10.1016/j.jnucmat.2006.05.031

target material or for a liquid target material under these conditions. Early in these technical discussions and analyses it was decided to utilize a liquid mercury target, which offered a number of advantages in power handling and neutronics. Also, in contrast to solid heavy metal targets the liquid metal target material does not suffer radiation damage in the usual sense. This choice was heavily influenced by the choice of a liquid metal target for the conceptual European Spallation Source (ESS) [4–6]. In the later sections of this paper materials work that was carried out in response to these early questions as well as to the most recent questions arising in the continually evolving knowledge in this field are described.

The Spallation Neutron Source (SNS) project is a partnership among Argonne National Laboratory (ANL), Brookhaven National Laboratory (BNL), Jefferson Laboratory (JLab), Lawrence Berkeley National Laboratory (LBNL), Los Alamos National Laboratory (LANL), and Oak Ridge National Laboratory (ORNL). International collaborations have been a very important aspect of the SNS project. In the target materials area, contacts and collaborations have been particularly intense with the European Spallation Source (ESS) concept studies, especially the design team at Forschungszentrum Jülich (FZJ), the Japan Proton Accelerator Research Complex (J-PARC) and the Schweizer Institüt für Nuklearforschung Quelle (SINQ) at the Paul Scherrer Institüt (PSI).

The SNS is located at ORNL in Oak Ridge, TN, USA, and managed by the ORNL SNS project office. The project is rapidly attaining completion. Building construction was finished in April 2005, and the full project will be completed in June 2006.

Groundbreaking took place in December of 1999, in which officials from US federal and Tennessee state governments took part with representatives of the US Department of Energy, the agency that is the official sponsor of the facility. Conceptual design of the SNS was completed in 1997 [7]. Figs. 1–3 show aerial views of the project atop Chestnut Ridge, which is a short distance from the ORNL main campus. Fig. 1 shows the site in March, 1999 prior to construction. It is interesting to relate the dates of the photographs in these figures to the meetings for the present series workshops. Fig. 1 corresponds to the year in which the IWSMT-3 was held. Three years later, in September 2002 the site had been cleared and early stages of construction were evident in a number of areas, as shown in Fig. 2. The foundation for the building that would house the target can be seen. This corresponds to the year in which the IWSMT-5 was held. In March 2005 the construction was nearing completion as shown in Fig. 3. The completed target

Fig. 1. Aerial view in March 1999 of the Chestnut Ridge location at Oak Ridge, Tennessee prior to the initiation of construction activities for the SNS.

Fig. 2. Progress of the SNS in September 2002. Site excavation, and building construction (labeled) are shown. The foundation for the target building can be seen.

Fig. 3. Aerial view of SNS in March 2005. Target building is visible in the middle ground.

building can be seen. The first target was installed there in June 2005, which date coincided with the present workshop (IWSMT-7).

Planned operation for the first five years is summarized in Fig. 4. Hours of operation devoted to user applications and accelerator physics are shown. Beam power is also projected together with reliability, defined as the percentage of time beam is available compared to the operational plan. At first, accelerator physics work will dominate the operational hours, transitioning to a user dominated operation after about two years. Beam power on target is expected to reach its full level after three to four years.

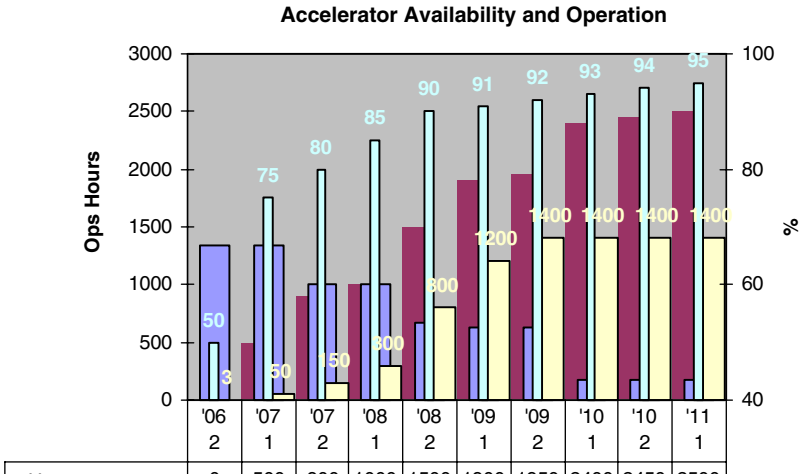

	'06 2	'07 1	'07 2	'08 1	'08 2	'09 1	'09 2	'10 1	'10 2	'11 1
User	0	500	900	1000	1500	1900	1950	2400	2450	2500
Accel.	1344	1344	1008	1008	672	624	624	168	168	168
Beam Power/kW	3	50	150	300	800	1200	1400	1400	1400	1400
Reliability (%)	50	75	80	85	90	91	92	93	94	95

Fig. 4. Planned operation of the SNS for the first five years. In the legend, 'User' denotes user operating hours (Ops) and 'Accel.' denotes accelerator physics work in hours.

2. Summary description

Protons are accelerated to energy of 1 GeV before impinging on the target to produce spallation neutrons. In turn these neutrons, which initially are of high energies and resemble a skewed fission spectrum containing a tail up to 1 GeV, are slowed to thermal energies in moderators adjacent to the target. The facility consists of an ion source, a linear accelerator, a proton storage ring, and a target station. Three sections comprise the linear accelerator, a drift tube linac (DTL), a coupled cavity linac (CCL) and a superconducting linac (SCL). At the end of the SCL the proton beam has attained energy of 1 GeV. A high energy beam transfer section carries the beam to the accumulator ring, where the beam is stored for about 1000 turns until enough protons are obtained to produce the desired on-target pulse. The beam is then transferred via a ring to target beam transfer section to the target station.

The target station includes the mercury target and associated circulation loop, neutron moderators and refrigeration systems, neutron beam lines and neutron scattering instruments, as well as a service hot cell for installing and removing targets and performing some sectioning operations on radioactive components [8]. The target is positioned within an iron and concrete shielding monolith. A sectioned representation of the monolith is shown in Fig. 5. The iron shielding radius is 5 m. The central region of the monolith, termed the inner reflector plug, is shown in Fig. 6. Table 1 gives a list of the key parameters for the target and mercury loop, including characteristics of the beam delivered by the accelerator system.

There are radiation effects issues for materials throughout the SNS. These include components in the tunnels of the accelerators and beam transfer lines, for example, such as magnets, electrical power supply components and electronic instruments. In addition there are three beam dumps, the Linac dump, the ring extraction dump and the ring injection dump. The latter is expected to operate continuously, absorbing up to 150 kW, and accumulating up to nearly 4 dpa per year of SNS operation (5000 h) at the front of the beam stop vessel [9]. Active cooling by means of a water loop is supplied for this dump because of the high power level. The other two dumps are expected to operate at less than 5% of the power of the ring injection dump, and will accumulate proportionally low radiation damage.

By contrast the mercury target container will accumulate about 21 dpa per SNS year [10,11]. In addition, it is subject to stress loads by the pulsed beam, contact with rapidly flowing mercury and, as will be discussed below most likely to cavitation

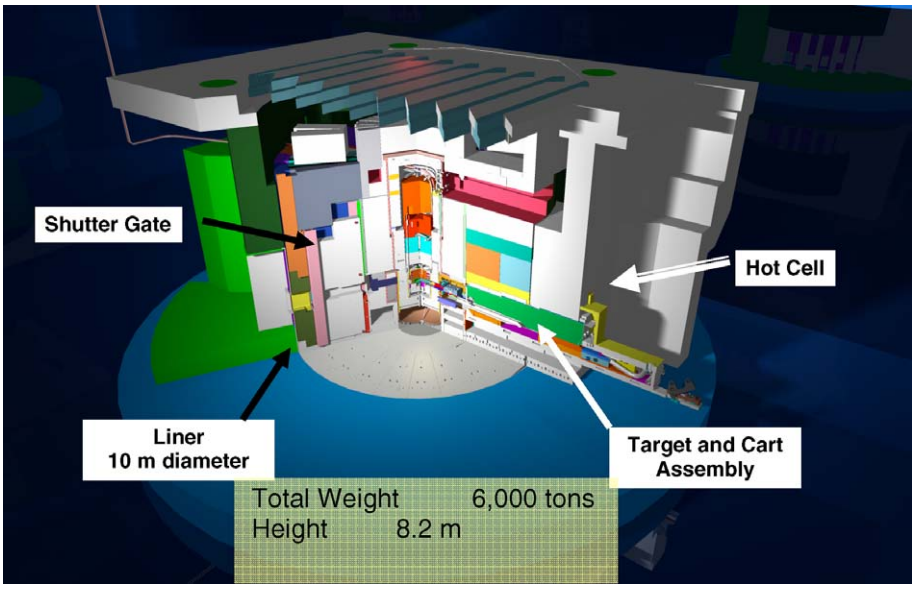

Fig. 5. Three-dimensional model of the target monolith showing locations of main components. The inner reflector plug is located at the center, with the target shown extending into it from the end of the target cart at right.

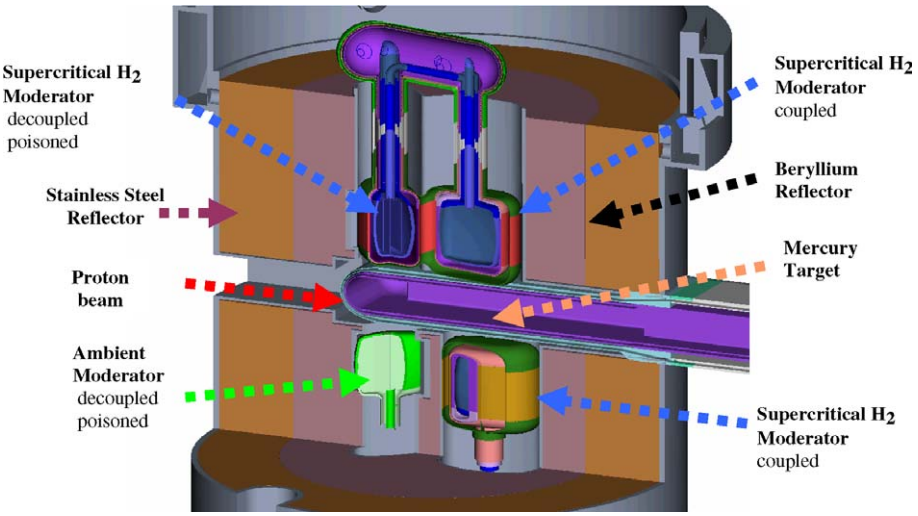

Fig. 6. Inner reflector plug main components. The structure of the central region of Fig. 5 is shown here, giving the locations of the mercury target, the four moderators and reflectors.

erosion. For these reasons it is deemed the most critical component to be considered with respect to materials-limited lifetime in this aggressive environment.

3. Materials R&D activities

Recent publications describe the structure of the spallation target module [12] and the 12 major types of experiments carried out to address materials issues in the target [13]. Broadly these experiments comprised five types of irradiation efforts, including spallation irradiations, irradiations in fission reactors, and ion irradiation experiments at a MeV triple-ion accelerator facility. The remaining experiments addressed cavitation erosion [14–16] and compatibility measures [17,18]. Irradiation was not included in these latter seven

Table 1
Key parameters for target and mercury loop

Beam energy	1 GeV
Power absorbed in Hg	1.2 MW
Pulse repetition rate	60 Hz
Pulse length	700 ns
Bulk mercury temperature	
Inlet to target	60 °C
Exit from target	90 °C
Mercury flow rate	340 kg/s
Mercury V_{max} (in window)	3.5 m/s
Total Hg inventory	1.4 m^3 (20 ton)
Mercury pumping power	30 kW
Max local Hg temperature	<200 °C
Hg target pressure	0.3 MPa

experimental efforts.[1] By means of this combination of work, recommendations for materials selection and a more complete picture of the expected performance of the target could be achieved. At the same time, however, there is no prototypical facility for the SNS conditions in operation, and therefore it was recognized that none of the work in the research and development program was fully prototypical of the operating facility. Under these circumstances the approach was to test individual and combined conditions by a variety of independent test methods so as to get as much information enveloping the target exposure conditions as possible. The papers published in a number of proceedings of recent meetings carry the information summarized here to much greater depth and detail [19–21].

The materials R&D program conducted in support of the SNS construction project is complete. It consisted of work in (1) radiation effects, (2) corrosion/compatibility with mercury for the target container material, and (3) mercury cavitation erosion of the container wall. Work has continued on cavitation erosion studies within a separately funded R&D effort on development for high power mercury targets. Summaries of the R&D work in these three areas are given in the remaining part of this manuscript.

[1] Strictly, the WNR experiments described in [14–16] and in a subsequent section of the present manuscript were exposed to radiation in the form of a pulsed proton beam, which induced sudden thermal expansion of the mercury and consequent cavitation erosion. However, the radiation did not provide a significant displacement damage dose to the materials of the experiment.

3.1. Radiation effects

Radiation effects activities include calculations of radiation damage and transmutations, covering displacement damage and the pka spectrum, helium, hydrogen, and heavier transmutants in both the target container material and in the mercury spallation target. The calculations for displacement damage, He and H are described in [10]. New mesh tally calculations have been carried out more recently to produce spatial maps of dpa, He and H transmutations in the target, moderator containers and reflector region [11]. The new calculations are in good agreement with the previous calculations. In the recent work the mesh tally method was modified to allow material-specific folding within MCNPX of cross sections with the calculated particle fluxes, whereas in the previous work the fluxes were tallied in MCNPX and later folded with cross sections using spreadsheets. The new work produces convenient visualizations of the radiation damage in the target-moderator-reflector regions of most interest. Figs. 7–9 show the results per SNS operating year (5000 h).[2]

Fig. 7 shows the calculated radiation damage in the target vessel in terms of dpa rate and helium production rate by transmutations. Fig. 8 shows the corresponding quantities for the top upstream moderator vessel. The three other moderators experience somewhat lower levels of damage. Fig. 9 shows the displacement damage for the reflector region near the target. Also shown in the latter figure are the displacements from neutrons and from protons separately. As expected, in the reflector most of the damage is from neutrons since this region is distant from the proton beam path. However, a small fraction of the damage can be seen to come from secondary or scattered protons.

An extensive experimental program of irradiations was carried out. It included spallation irradiations in the LANSCE beamstop area in the LASREF facility similar to the irradiations described in [22,23]; irradiations in the target of the SINQ [24]; fission reactor irradiations; and ion beam irradiations with single ion beams or combinations of multiple ion beams. Many of the results have been published in the proceedings of the IWSMT workshops referred to earlier in this

[2] Note that the results in Figs. 7–9 are presented in dpa or appm He per SNS operating year (5000 h), whereas the previous work in [10] gave results for a full year (8760 h).

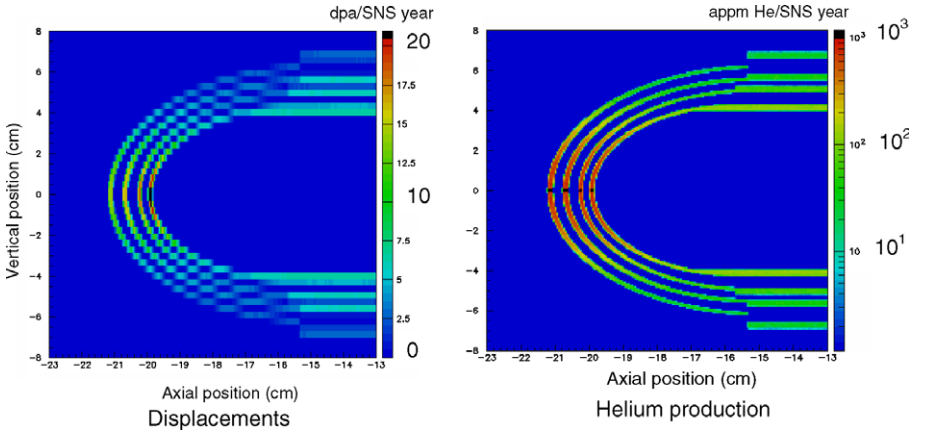

Fig. 7. Spatial map of displacement damage (dpa) shown at left and helium transmutation (appm He) shown at right in the front portion of the 316 LN stainless steel target module of the SNS. The inner two walls (smallest radii) form the mercury target vessel and the outer two walls are the water cooled shroud. The maximum displacement damage is approximately 21 dpa and maximum helium production is approximately 800 appm.

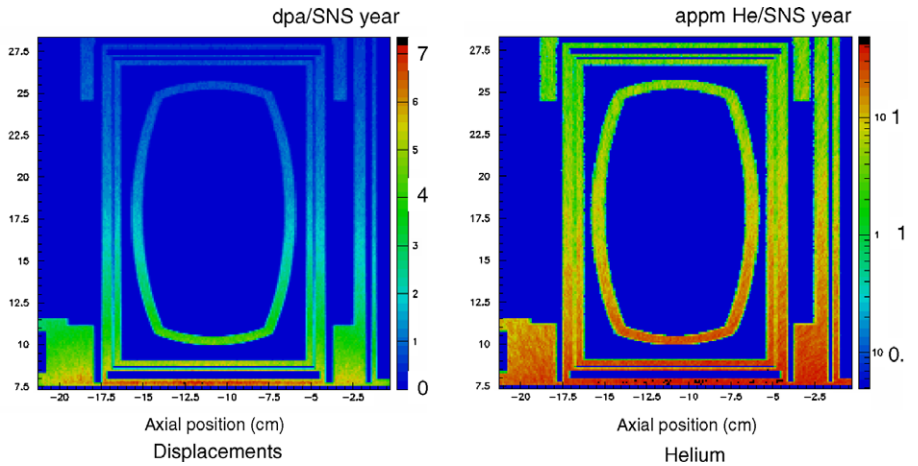

Fig. 8. Displacement damage (dpa) shown at left and helium transmutation (appm He) shown at right in the aluminum alloy 6061 top upstream neutron moderator. The maximum displacement damage is less than 8 dpa and the helium production is less than 50 appm.

section, and because it would be impractical to show a representative summary of all these results here, the reader is referred to those proceedings.

One significant highlight of some of these results is shown in Fig. 10 [25]. The figure plots the yield stress and ductility in tensile tests of a number of irradiated stainless steels as a function of dose. Steels irradiated both in spallation facilities and in fission reactors are shown. For the fission reactor irradiations many of the data points have been obtained by the US fusion materials program [26]. Those latter data are more numerous than indicated here, however, only the points corresponding to temperatures <200 °C, considered relevant to the SNS target, are shown in the figure (pale diamonds). These provide a backdrop and field of comparison for results obtained in the SNS R&D program and in related work under spallation conditions (all of the other points). From the figure it can be seen that the yield stress and ductility both change in a gradual manner with increasing dose. The exception is the 316 L data obtained by LANL for irradiations in the LASREF [23]. For the 316 L ductility loss was relatively rapid and the ductility reached very low values after only a few dpa. All of the other data lie within the envelope obtained from the band of the fission reactor data. In particular, the data for 316 LN obtained in spallation

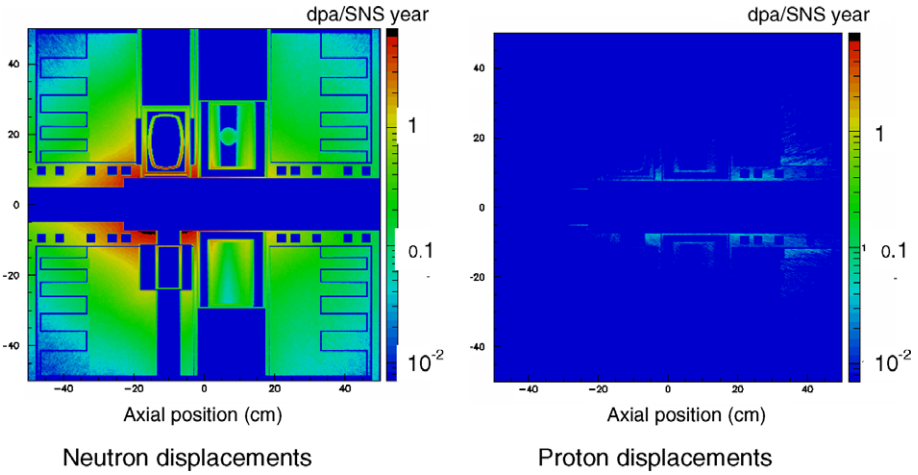

Fig. 9. Displacement damage (dpa) in the reflector region surrounding the target. The maximum displacement rate is ~7 dpa in Al 6061, and lower in steel and Be. On the left is shown the displacement production from neutrons and on the right is the displacement production from protons. The maximum He production, not shown in the above maps, is ~40 appm in Al 6061 and ~30 appm in Be.

irradiations and in fission reactor irradiations showed a trend indicating that several percent ductility remained after irradiations to more than 10 dpa. In earlier work 316 LN stainless steels also had shown better post-irradiation fracture toughness than other stainless steels at the lower temperatures relevant to SNS [27].

3.2. Corrosion

An extensive program of tests was conducted to investigate whether stainless steels, and in particular type 316 LN, would suffer corrosion in mercury. A reasonable concern was that nickel, a major constituent in the steel, might be removed to some extent since it is known to be soluble in mercury at higher temperatures. Experiments were therefore carried out in stagnant mercury, and in flowing mercury in both thermal convection loops and in a pumped flow loop. The results can be summarized to say that no significant corrosion was observed [28].

In the thermal convection loops the conditions were deliberately made more extreme than in the application case. The temperature of the test was higher, to encourage the Hg wetting of the steel, typically the hot leg temperature was 305 °C, and ΔT to the cold leg was set to 60 °C. Tests were run for durations up to 5000 h. In the worst case the depletion of the surface extended to about 15 μm, and wetting of coupons was observed only in certain cases. In the thermal convection loops the flow rates were approximately 1 m/min. To answer the question of whether a more prototypical flow velocity of order 1 m/s would make a difference, tests of corrosion coupons were carried out in a pumped flow loop. In tests of approximately 1000 h duration virtually no corrosion was detected. In those tests the hot leg was again at a higher temperature than the application, 250 °C. The ΔT to the cold leg was 150 °C. No apparent wetting by Hg was observed and no attack of the 316 LN surfaces could be detected. Metallography revealed negligible surface roughness changes from the initial state. All of these results can be summarized to say that good compatibility with Hg was demonstrated in these tests. A significant question that remains is whether the presence of the high intensity mixed particle irradiation field in the SNS target would affect wetting or other compatibility processes.

3.3. Mercury effects on mechanical properties

Three types of testing of increasing severity were conducted to investigate whether mercury would have an effect on mechanical properties of 316 LN stainless steels and some additional materials of interest. In the earliest tests, static U-bend specimens were immersed in mercury after the specimens were initially bent beyond yield and then held at stress by a mechanical fastener. No effect could be found on the materials immersed in mercury compared to control specimens in air. Tensile tests were then performed in mercury and air. Most of the tests were carried to failure as in normal tensile testing.

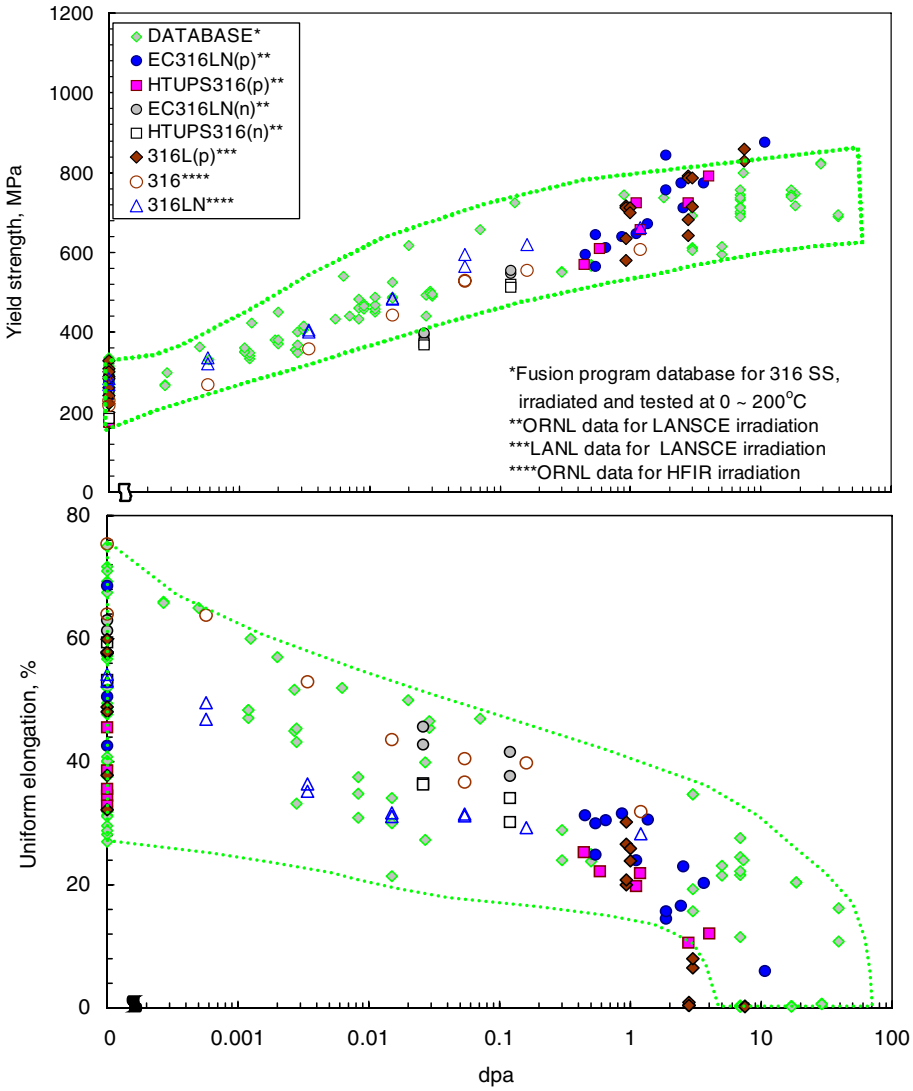

Fig. 10. Yield strength and uniform elongation obtained in tensile tests of irradiated austenitic stainless steels. Pale diamonds are points obtained previously in fission reactor irradiations [26]. All of the other points were obtained from spallation materials research programs. The parenthetical (n) and (p) in the legend indicate the general location of the specimens in irradiations at LASREF: the former were downstream of the spallation target and were irradiated with both protons and neutrons; the latter were upstream of the spallation target and were irradiated primarily by the incident 800 MeV protons. (For interpretation of the references in color in this figure legend, the reader to the web version of this article.)

However, a hold time was introduced into other tests because it was suspected the mercury could possibly enter small surface cracks or defects and lead to crack growth. Therefore some tests were stopped and held at stress after the yield stress was exceeded but before the ultimate tensile failure stress was applied. Then after several weeks the tests were continued to failure. In all these tests, no significant differences in yield stress, ultimate tensile stress or uniform elongation could be attributed to mercury when compared to corresponding tests in air [29].

An extensive program of fatigue testing was conducted over several years. For a fairly wide range of parameters, full fatigue curves were generated for stress amplitude versus cycles to failure. The results of tests in mercury and in air were compared for wide ranges of frequencies and *R*-ratios (maximum to minimum stress amplitude ratios). Several tests were done with different applied load waveforms.

Most work was carried out under load control conditions, but some tests were also performed under strain control in order to compare with earlier work. Complete documentation of the fatigue testing program is available [30].

Part of this data is shown in Fig. 11 for tests in the range of 0.1–10 Hz in both mercury and air. In this figure an apparent effect of mercury can be seen in shortening the fatigue life at high alternating stresses and low frequencies in the range 0.1–1 Hz. At lower stresses and for a frequency of 10 Hz there is no apparent effect of mercury. Other tests performed at frequencies up to 700 Hz similarly show no effect of mercury at low stresses or on the endurance limit.

Fig. 12 shows the results for tests conducted for a range of R ratios. R ratio of -1 denotes a push–pull test of equal tension and compression. Positive R values indicate a mean tensile condition for the entire fatigue cycle, and could be considered to be more damaging in an aggressive environment. The straight line (Goodman) or parabola (Gerber) are often used to estimate the results of failure stress for R ratios between $R = -1$, fatigue strength for fully reversing stress, and $R = 1$, ultimate tensile failure stress for constant applied stress. The region falling to the right of the line and especially to the right of the parabola can be considered to be a safe region, i.e., failure in an actual application falling in this range would be at a higher stress than predicted by connecting the two extreme points for $R = -1$ and $R = 1$. To confirm that the material in mercury would indeed fail in this expected region, tests were conducted at several positive R ratios ranging from 0.1 to 0.75. All points lay to the right of the line and two were to the right of the parabola. Although all R ratios could not be tested, these discrete points suggest that in both air and in mercury the 316 LN will perform better than the minimum estimation (Goodman line).

3.4. Cavitation erosion

As summarized in Table 1, the proton beam is pulsed with duration of 0.7 μs and a repetition rate of 60 Hz. Cavitation erosion may be caused by the rapid and intense energy input when these beam pulses are absorbed in the mercury. The thermal expansion following the rapid heating that ensues gives rise to pressure waves. These pressure waves propagate at the speed of sound to the vessel walls and are followed by rarefactions. In these regions of tensile stress the (low) tensile strength of the liquid is exceeded and the mercury breaks apart or cavitates. Cavitation bubbles form throughout the mercury. Their subsequent collapse in the hydrostatic compressive stress of the following pressure wave cycles can produce small erosion pits in the container wall. The mechanisms that produce the pitting erosion are generally thought to involve

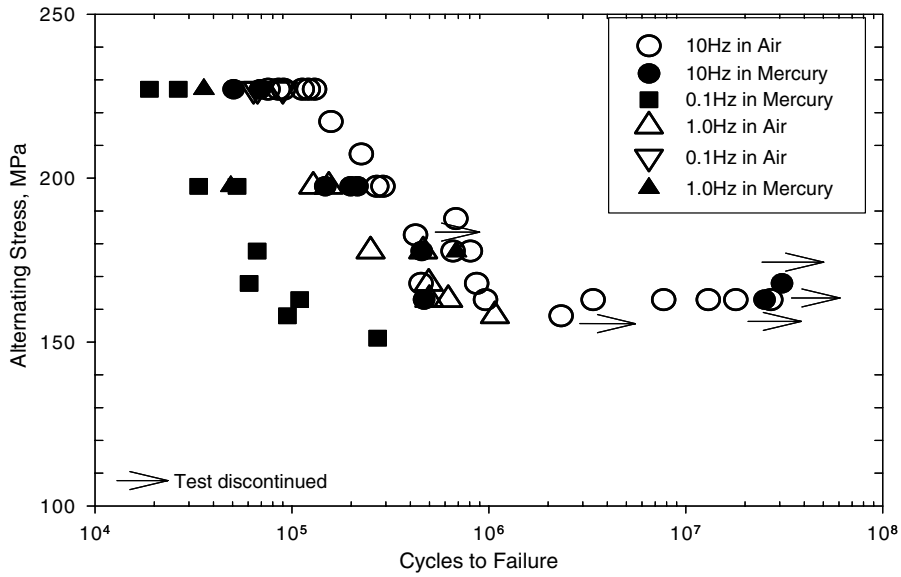

Fig. 11. Alternating stress vs cycles to failure for tests performed on 316 LN stainless steel near room temperature in static mercury and in air. Cycle frequency ranged from 0.1 to 10 Hz at R ratio of 0.1.

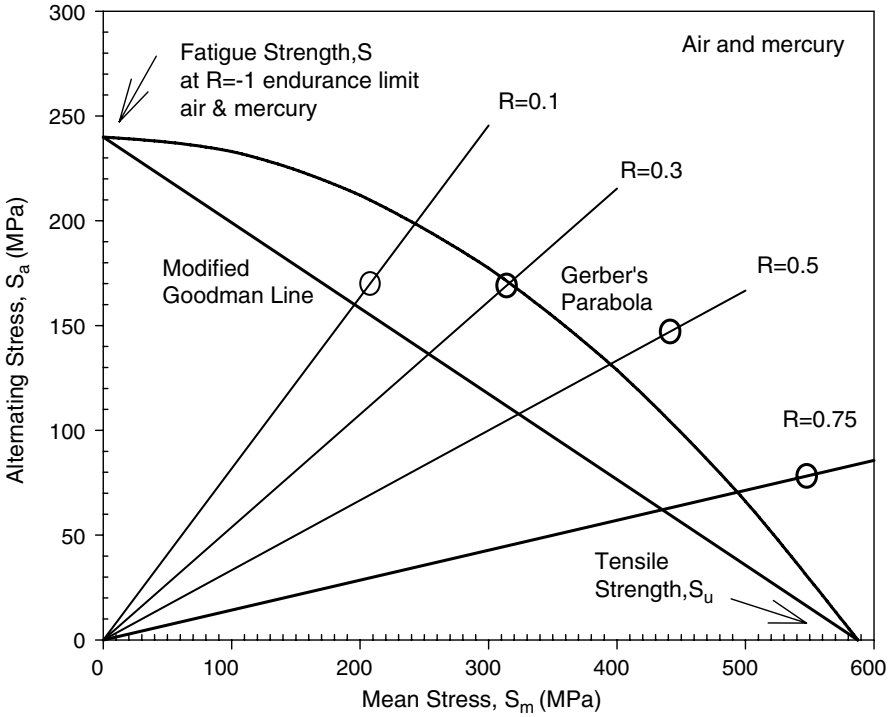

Fig. 12. Results of fatigue tests to a constant fatigue life for a range of different R ratios in air and mercury. The points indicate the results of the tests. The lines connecting the fatigue strength for full stress reversal to the tensile strength are accepted correlations for normal performance.

the high pressure microjets and localized shock waves originating in the asymmetrically collapsing bubbles, by analogy to earlier more basic work on cavitation erosion by bubble collapse in a water environment [31,32].

As described in [14] tests conducted early in the SNS target development program had shown that mercury, with the level of impurities and dissolved gases expected in the SNS process loop, will cavitate when the tensile pressure reaches only a few atmospheres.

Erosion due to short-pulse beam deposition was first observed in ISOLDE molten metal targets [33]. Early SNS cavitation erosion studies conducted using an ultrasonic horn, showed that damage with mercury was much more severe than with water at the same power level, but it was not clear how to interpret these results in view of the vastly different pressure and frequency regimes present with the ultrasonic horn tests compared to the actual SNS conditions [34]. More recently, a team of researchers at the Japan Atomic Energy Research Institute (JAERI) observed pitting of stainless steel surfaces that were in contact with mercury subjected to large mechanically induced pressure pulses of the same magnitude as those expected at full power pulses in SNS [35]. In view of the JAERI results, targets used in pulsed proton beam experiments at the Los Alamos Neutron Science Center (LANSCE) Weapons Neutron Research (WNR) facility, designed to examine wall stresses in simulated SNS targets, were examined. However, because no pre-test inspections had been performed, it was not possible to distinguish between beam-induced pits and other imperfections in the surface of the materials.

Subsequently, new tests were designed specifically for investigating pitting in mercury in response to proton beam pulses. In parallel, a number of additional tests using mechanical energy inputs instead of proton beam pulses were developed. These laboratory devices included a collaboration using a magnetic impact test machine (MIMTM) designed and operated by JAERI, a gravity-driven drop test device at ORNL and an ultrasonic horn at ORNL. The latter was designed to be similar to a standard method [36] used for testing cavitation behavior of materials in water. In the WNR tests

and in all of these laboratory tests, cavitation erosion was produced to varying degrees depending on the parameters of the tests. In particular, tests in the energy density range of beam pulses for SNS showed cavitation erosion. Many of these test apparatuses and the results of some of their respective experiments are documented in the proceedings of the earlier workshop in this series [37]. The most recent test results from the JAERI work are reported in a paper contained in the present proceedings [38].

Fig. 13 shows the calculated energy deposition during a SNS proton pulse. The peak energy deposition is approximately 13 MJ/m^3. Although the calculated peak temperature rise in mercury for one pulse is below 10 °C, the rate of rise is about 10^7 °C/s. The energy deposition is an isochoric process, since the energy deposition time, 0.7 μs, is much less than the time required for the mercury to expand in response to the increased temperature. Calculations show that it takes about 33 μs for a pressure wave propagating at the speed of sound in mercury to traverse a length equal to the proton beam lateral dimension. Local pressure in this pulse is two orders of magnitude higher than the ambient static pressure in the flowing mercury (34 MPa vs 0.3 MPa). Fig. 14 is a micrograph obtained by scanning electron microscopy (SEM) on one of the 316 LN stainless steel diaphragms subject to proton beam pulsed at the LANSCE–WNR.

Fig. 15 presents a summary of mean depth of erosion for the LANSCE–WNR proton beam tests, together with the three types of tests described above that employ mechanical energy inputs. Only the ultrasonic horn tests, which operate at 20 kHz, could produce a number of cycles equal to or greater than the reference for the SNS target operated for several weeks. The MIMTM results delivered a number of cycles lower but within the same order of magnitude as the reference. The drop tests were at best two orders of magnitude below the reference. The WNR tests gave results for only 100–1000 cycles. These results were extrapolated to estimate the mean depth of erosion in the SNS target for a given number of cycles. Because the 100-pulse damage for MIMTM was slightly worse than the corresponding proton pulse damage, and, when extrapolated by an order of magnitude, substantially worse than the ultrasonic horn damage for the same material, the MIMTM results were chosen for this extrapolation. From these results we can conclude that the mean depth of erosion in the SNS target was within an

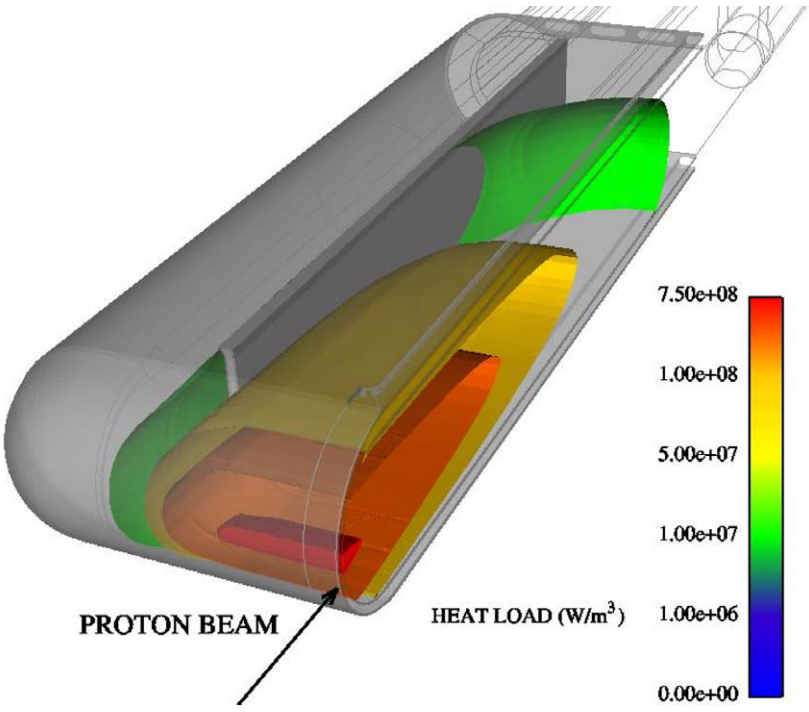

Fig. 13. Calculated input energy density in the SNS target from a proton beam pulse.

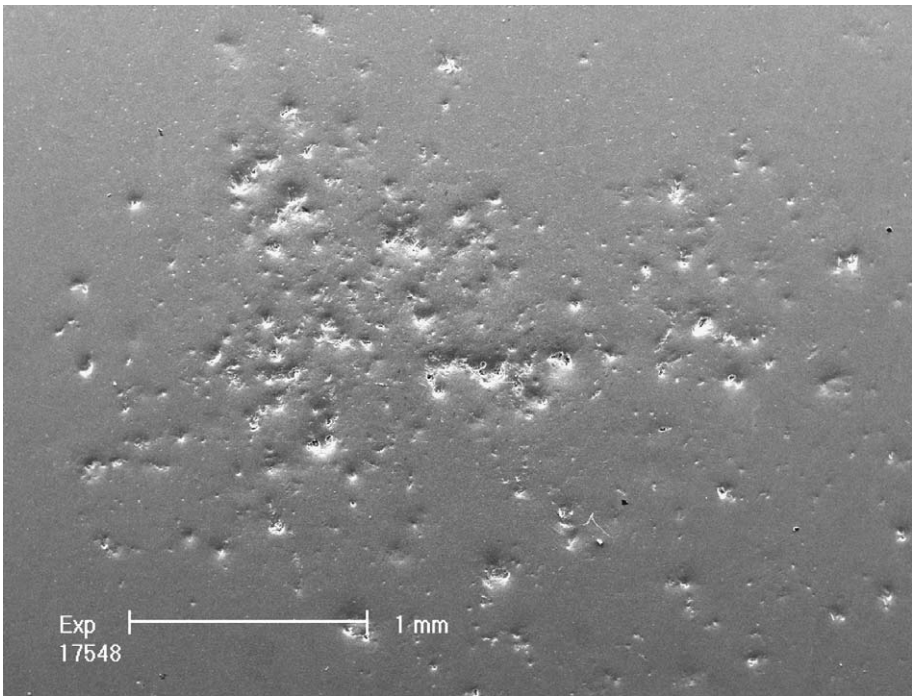

Fig. 14. Scanning electron micrograph of type 316 LN stainless steel diaphragm exposed to 100 proton beam pulses at the LANSCE–WNR.

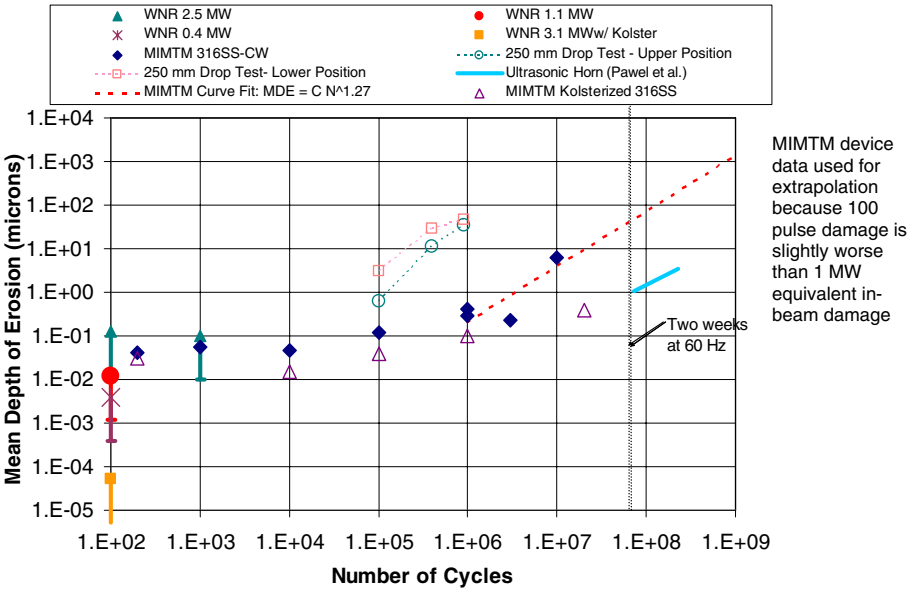

Fig. 15. Mean depth of erosion vs cycles for proton beam pulse tests, together with results from laboratory tests where energy pulses were created by mechanical means: WNR denotes proton beam tests at the LANSCE accelerator at the indicated SNS-equivalent energy densities; MIMTM denotes results from the JAERI impact tests; drop test results and ultrasonic horn test results from ORNL are shown as indicated in the legend. Material was 316 LN stainless steel cold worked to between 20% and 50%, with surface carburized (Kolsterized) in one case.

allowable level for up to two weeks of operation at 1 MW, which was the minimum level of mercury target lifetime deemed to be acceptable for SNS operation with the current target design [14].

It should be pointed out, however, that there are numerous uncertainties regarding cavitation erosion in the SNS. Firstly, it has not been proven that the SNS target will experience these levels of erosion, since a prototype test has not been available. The levels in the SNS could be lower or higher. The tests represented in Fig. 15 simulate aspects of the operating parameters, but do not reproduce such features as the geometry, flow conditions and the large volume heat transfer loop associated with the actual target. In addition, how the incubation number of cycles for significant erosion damage depends on power level and pulse frequency, for example, is not understood. Similarly, although mean depth of erosion is a sensible measure to apply, it is not the only measure of erosion damage that may be relevant. Recently, there has been progress in characterizing these behaviors [38]. The questions relating to behavior in prototypical geometries and loop conditions will only be answered in the operation of the SNS.

4. Future work

At the present time, and with significant uncertainties because a prototype facility is not available, the cavitation erosion problem is expected to be the lifetime limiting phenomenon for the target module. For the immediate future, more research and development is planned on the pitting issue. New experiments were recently conducted, during the same timeframe as the present workshop, on cavitation erosion at the LANSCE–WNR. These experiments differed from those described above in that circulating mercury in a small pumped loop was exposed to the proton beam in the most recent experiments, whereas the earlier experiments employed small targets containing stagnant mercury. In addition, in the recent experiments a population of helium bubbles was introduced. In principle the volume of these bubbles was expected to help accommodate the sudden volume expansion of the mercury after it absorbed the thermal energy deposited by a proton beam pulse. In a macroscopic sense then, the bubbles should make the mercury more compressible, and therefore not as damaging to the container wall as a more rigid liquid not containing bubbles. The specimens from these experiments will be examined in the near future to confirm these speculations.

Follow up work on cavitation will include more precise methods to generate and maintain bubble populations of the desired size distribution, together with bubble diagnostic techniques to monitor the bubble distributions. New experiments will be conducted to confirm pitting damage mitigation and to develop higher cycle laboratory tests that reproduce aspects of the low cycle proton beam pulse tests. Simulation methods will also be pursued to improve understanding of pitting damage and bubble behavior. Experimental validation and the resulting confidence in such simulation methods will permit predictions for materials pitting damage for conditions where there are no experimental data. Such methods would be valuable for projecting cavitation erosion for a full range of beam powers, for example.

As engineering solutions for pitting are developed through the course of the above research, and the cavitation erosion lifetime is extended, then other phenomena will become lifetime limiting. Chief among these is expected to be radiation induced embrittlement. As described earlier, type 316 L stainless steel in spallation irradiations showed essentially complete loss of uniform elongation at doses below 5 dpa. Type 316 LN performed better, maintaining some degree of ductility to doses beyond 10 dpa under spallation conditions. We have recommended type 316 LN stainless steel as the material from which to fabricate the SNS mercury target module. However, hardening and loss of ductility of a material should not be considered in isolation. The context of the service application is very important. There are numerous examples where severely embrittled alloys can continue to perform their functions in various nuclear applications. The key consideration is whether or not there is potential for application of a load with a magnitude or loading rate that will challenge the compromised material properties. For evaluation in this broader context, we must consider the combined influences of displacement damage and transmutations together with such issues as (1) dynamic loads and the associated fatiguing of irradiation hardened material, (2) contact with mercury and the associated corrosion or liquid metal embrittlement processes in the presence of irradiation, and (3) pitting damage to irradiated material and its possible consequences for crack initiation in a highly hardened material under mechanical loads.

Acknowledgements

The target materials R&D program benefited from the work of a large team with numerous indi-

vidual contributions. In particular, we thank Drs T.S. Byun, J.R. DiStefano, K. Farrell, P.D. Ferguson, J.D. Hunn, S.J. Pawel, B.W. Riemer, J.P. Strizak, and M.S. Wechsler. The SNS is sponsored by the Office of Science, US Department of Energy, under Contract No. DE-AC05-00OR22725 with UT-Battelle, LLC.

References

[1] H. Ullmaier, F. Carsughi, Nucl. Instrum. and Meth. B 101 (1995) 406.
[2] W.F. Sommer, T.O. Brun, L.L. Daemen, L.S. Schroeder, Materials for Spallation Neutron Sources, Los Alamos National Laboratory, 1995.
[3] L.K. Mansur, H. Ullmaier, (Eds.), Proceedings of the International Workshop on Spallation Materials Technology, Oak Ridge, TN, 23–25 April, CONF-9604151, 1996.
[4] G.S. Bauer, et al., (Eds.), The ESS Technical Study, vol. III of The European Spallation Source Study, The ESS Council (1996) ESS-96-53-M, ISBN 090 237 659.
[5] H. Lengeler, The European Spallation Source Study (ESS), in: Proceedings of the ICANS-XIII Conference, PSI Proceedings 95-02, ISSN 1019-6447, 1995, p. 819.
[6] B.R. Appleton, G.S. Bauer, in: Proceedings of the International Workshop on the Technology and Thermal Hydraulics of Heavy Liquid Metals, Schruns, Austria, 24–29 March, 1996, Oak Ridge National Laboratory Report, CONF-9603171, June 1996.
[7] The National Spallation Neutron Source Conceptual Design Report, Oak Ridge National Laboratory Report, NSNS/CDR-2/V1 and NSNS/CDR-2/V2, May 1997.
[8] T.A. Gabriel, J.R. Haines, T.R. McManamy, J. Nucl. Mater. 318 (2003) 1.
[9] F.X. Gallmeier, Draft: Neutronics Calculations in support of the ring injection dump design, Spallation Neutron Source Report SNS-106100200-DA000?-R00, March 2005, Oak Ridge, TN.
[10] M.H. Barnett et al., J. Nucl. Mater. 296 (2001) 54.
[11] P.D. Ferguson et al., Radiation damage calculations for the SNS target, moderator vessels, and reflector system, in: Proceedings of the Twelfth International Symposium on Reactor Dosimetry, 8–13 May, 2005, Gatlinburg, TN, USA, American Society for Testing and Materials, West Conshohocken, PA, USA.
[12] L.K. Mansur et al., J. Nucl. Mater. 296 (2001) 1.
[13] L.K. Mansur, J. Nucl. Mater. 318 (2003) 14.
[14] J.R. Haines et al., J. Nucl. Mater. 343 (2005) 58.
[15] B.W. Riemer et al., J. Nucl. Mater. 318 (2003) 92.
[16] J.D. Hunn, B.W. Riemer, C.C. Tsai, J. Nucl. Mater. 318 (2003) 102.
[17] S.J. Pawel, J.R. DiStefano, L.K. Mansur, K. Farrell, J.P. Strizak, T.S. Byun, Compatibility and radiation damage tests in support of the SNS, in: Proceedings of the Topical Winter Meeting on Accelerator Applications, held at the American Nuclear Society Meeting, Long Beach, California, 14–18 November, American Nuclear Society, La Grange Park, IL, 1999, p. 117.
[18] J.P. Strizak et al., J. Nucl. Mater. 343 (2005) 134.
[19] M.S. Wechsler, L.K. Mansur, C.L. Snead, W.F. Sommer (Eds.), Proceedings of the Symposium on Materials for Spallation Neutron Sources, held at the TMS Annual Meeting, Orlando, Florida, 9–13 February, 1997, The Minerals, Metals and Materials Society, Warrendale, PA, 1998.
[20] Y. Dai et al. (Eds.), Proceedings of the 4th International Workshop on Spallation Materials Technology, (IWSMT-4), Schruns, Austria, 8–13 October, 2000, J. Nucl. Mater. 296 (2001) 1.
[21] L.K. Mansur et al. (Eds.), Proceedings of the 5th International Workshop on Spallation Materials Technology, (IWSMT-4), Charleston, South Carolina, USA, 19–24 May, 2002, J. Nucl. Mater. 318 (2003) 1.
[22] W. Sommer et al., Mater. Character. 43 (1999) 97.
[23] S. Maloy et al., J. Nucl. Mater. 318 (2003) 283.
[24] Y. Dai et al., J. Nucl. Mater. 343 (2005) 33.
[25] T.S. Byun et al., J. Nucl. Mater. 303 (2002) 34.
[26] J.E. Pawel et al., J. Nucl. Mater. 239 (1996) 126.
[27] A.A. Tavassoli, Fus. Eng. Des. 29 (1995) 371.
[28] S.J. Pawel, J.R. DiStefano, E.T. Manneschmidt, J. Nucl. Mater. 296 (2001) 210.
[29] S.J. Pawel, et al., Screening test results of fatigue properties of type 316 LN stainless steel in mercury, Oak Ridge National Laboratory Report, ORNL/TM-13759, March 1999, Oak Ridge, TN, USA.
[30] J.P. Strizak, H. Tian, P.K. Liaw, L.K. Mansur, Fatigue properties of type 316 LN stainless steel in air and mercury, Spallation Neutron Source Report, SNS-101060200-TD0001-R00, 91 pages, February 2003, Oak Ridge, TN, USA.
[31] Y. Tomito, A. Shima, J. Fluid Mech. 169 (1986) 535.
[32] A. Philipp, W. Lauterborn, J. Fluid Mech. 361 (1998) 75.
[33] J. Lettry, R. Catherall, P. Drumm, A. Evensen, O. Jonsson, E. Kugler, J. Ober, J.C. Putaux, J. Sauvage, H. Ravn, M. Toulemonde, the ISOLDE Collaboration, in: Proceedings of the 13th Meeting of the International Collaboration on Advanced Neutron Sources (ICANS-XIII), 11–14 October, Villigen, Switzerland, 1995.
[34] M.D. Kass, J.H. Whealton, N.E. Clapp, J.R. DiStefano, J.H. DeVan, J.R. Haines, M.A. Akerman, T.A. Gabriel, Tribol. Lett. 5 (1998) 231.
[35] M. Futakawa, H. Kogawa, R. Hino, J. Phys. IV France 10 (2000) 247.
[36] Standard test method for cavitation erosion using vibratory apparatus, ASTM G-32-98, American Society for Testing and Materials, Philadelphia, PA, 1998, p. 109.
[37] K. Kikuchi, H. Kogawa, M. Futakawa, S. Ishikura, M. Kaminaga, R. Hino, J. Nucl. Mater. 318 (2003) 84.
[38] M. Futakawa, T. Naoe, H. Kogawa, Y. Ikeda, Degradation of fatigue strength by pitting damage, this workshop IWSMT-7.